/N-63

NASA Technical Paper 3700

Design of Life Extending Controls Using Nonlinear Parameter Optimization

Carl F. Lorenzo
Lewis Research Center, Cleveland, Ohio

Michael S. Holmes and Asok Ray
Pennsylvania State University, University Park, Pennsylvania

National Aeronautics and
Space Administration

Lewis Research Center

April 1998

Trade names or manufacturers' names are used in this report for identification only. This usage does not constitute an official endorsement, either expressed or implied, by the National Aeronautics and Space Administration.

Available from

NASA Center for Aerospace Information
800 Elkridge Landing Road
Linthicum Heights, MD 21090-2934
Price Code: A03

National Technical Information Service
5287 Port Royal Road
Springfield, VA 22100
Price Code: A03

Design of Life Extending Controls Using Nonlinear Parameter Optimization

Carl F. Lorenzo
National Aeronautics and Space Administration
Lewis Research Center
Cleveland, Ohio

Michael S. Holmes and Asok Ray
Pennsylvania State University
University Park, Pennsylvania

Summary

This report presents the conceptual development of a life extending control system where the objective is to achieve high performance and structural durability of the plant. A life extending controller is designed for a reusable rocket engine via damage mitigation in both the fuel and oxidizer turbines while achieving high performance for transient responses of the combustion chamber pressure and the O_2/H_2 mixture ratio. This design approach makes use of a combination of linear and nonlinear controller synthesis techniques and also allows adaptation of the life extending controller module to augment a conventional performance controller of a rocket engine. The nonlinear aspect of the design is achieved using nonlinear parameter optimization of a prescribed control structure.

1. Introduction

Systems with high performance requirements and high power densities such as the Space Shuttle Main Engine (SSME), hypersonic propulsion engines, and gas turbine engines often have a small number of critical components that operate close to mechanical design limits. The critical components are also indicators of the effective lifetime of the entire system. These components often experience maximum stress conditions during transients, and it is during such transients that large decrements in the component life are experienced. Possible damage modes include spalling, creep, corrosion, and fatigue. Simply minimizing stress levels is *not* always a solution to these problems because it will typically result in an excessive loss of dynamic performance.

The effect of thermal transient loading on the Space Shuttle Main Engine (SSME) turbine blades during startup and shutdown is a typical example of the above scenario. It was against the backdrop of the durability problems of the SSME that the concept of life extending control (LEC) has evolved. The fundamental concept of life extending control is to control the rates of change and operating domains of some performance variables to minimize damage (or damage rates) of the critical components while simultaneously maximizing the dynamic performance of the plant. While the life extending control technology was developed initially for the SSME, it has broad application to many situations where both rapid response through transients and long life are required.

The fundamental concept of life extending control has been forwarded by Lorenzo and Merrill (1991a and 1991b). The following basic approaches have been considered: (1) implicit life extending controls, which use current cycle based damage laws, and (2) direct life extending controls which assume the development of a continuous form of damage law. The availability of a continuum damage model allows a more straightforward development of the life extending control concept and, hence, a simpler implementation. In the life extending control implementations that have been considered, in addition to the plant and the performance controller, a structural estimator must be addended which provides the stress, strain, and temperature states of the critical components. These are used by an appropriate continuum damage model which in turn provides estimates of the current damage rates for the damage controller. A continuum fatigue damage model based on the local stress method has been developed by Lorenzo (1994).

Ray et al. (1994a and 1994b) have shown that, in an open-loop setting, it is possible to reduce the fatigue damage rate and accumulation in the turbine blades of a reusable rocket engine (e.g., the space shuttle main engine) with little sacrifice in plant performance. Their damage reduction procedure, however, is based on an extensive off-line optimization and does not take advantage of on-line damage predictions or measurements. Also, the resulting feedforward signal is optimized for a particular set of initial conditions and a maneuver which must be specified *a priori*. This method may not be applicable to maneuvers and/or initial conditions not used in the optimization procedure. Dai and Ray (1996) applied the same procedure to creep damage in the main thrust chamber wall of the same rocket engine.

Kallappa et al. (1997) find an optimal open-loop control sequence which mitigates the creep and fatigue damage being accumulated in the main steam header of a fossil-fueled powerplant. The feedforward control is augmented with a feedback controller to provide robustness to the system.

Tangirala (1996) applies a combined feedforward/feedback controller synthesis methodology to a laboratory testbed. The synthesis procedure involves finding an optimal open-loop input sequence and augmenting it with a damage-mitigating output feedback controller. In a similar manner, Holmes, Tangirala, and Ray (1997) present a procedure for designing output feedback damage-mitigating controllers for a reusable rocket engine.

Holmes and Ray (1997) use a fuzzy controller to mitigate damage in the turbine blades of a reusable rocket engine. A similar procedure is applied to a fossil-fueled powerplant in Holmes (1997).

The approach taken in this report is to separate the design of the performance controller and the damage controller. That is, an aggressive performance controller is designed using standard (linear) techniques to achieve a high level of dynamic response for the plant, here a reusable rocket engine. Following this, the structure for the life extending control is added as an outer loop. It consists of a structural estimator, followed by a continuum damage model, in turn followed by a linear controller. The parameters of the linear control structure are then determined using nonlinear parameter optimization. The expected benefits of such an approach are the following: (1) the process is straightforward to apply, (2) it eliminates the necessity for determining the optimal open-loop response, and (3) it should be applicable to any form of input command desired.

This report is organized into eight sections including the Introduction. In Section 2 a high level view of the life extending control system is presented. A description of the reusable rocket engine used in this study is given in Section 3. The damage model used to calculate fatigue damage in the turbine blades is presented in Section 4. Section 5 contains details on the design of the performance controller, and Section 6 describes the damage controller design procedure. Computer simulation results are presented in Section 7, and the summary of the research and conclusions are given in Section 8.

2. The Life Extending Control System

The Life Extending Control (LEC) system functions as an integral part of the primary control loop, sometimes within the hierarchical structure of the intelligent control system (Lorenzo and Merrill,1991a and 1991b). The focus of this section is on the fundamental issue of formulating a control structure for the LEC system with the objective of optimizing simultaneously the plant dynamic performance and minimizing the accumulated damage and/or damage rate in critical plant components. Figure 2.1 shows a conceptual view of the LEC system. The high-level philosophy taken in this report is to develop an LEC system control approach that can easily be addended to a conventional performance controller design.

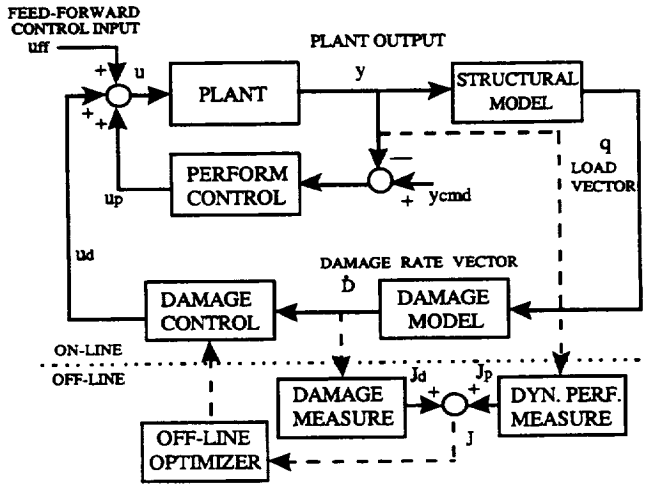

Figure 2.1. - Schematic diagram of Life Extending Control system and off-line optimizer.

The approach taken here is to design an aggressive performance controller to achieve a high level of dynamic performance. In the typical situation, with a linear or (linearizable) plant, the performance controller is designed using any of a number of linear controller design techniques (such as H_∞, μ synthesis, etc.). This assures stability in the inner loop with good dynamic performance as a starting point for the design of the highly nonlinear outer loop. This system of plant plus performance controller then becomes an augmented plant around which the life extending control loop is added. The essential elements of this outer loop are (1) a structural estimator that uses a set of plant outputs to estimate the load conditions (stress, temperature, or strain at the critical locations), (2) a damage model that uses these conditions to determine the rate of damage in the critical location, and (3) the damage controller. The damage model is a continuum time (as opposed to cycle) based representation of the damage so that it can be incorporated in the real time application.

The objective is to reduce the damage rate and the accumulated damage at the critical points of the structure during transients where the time-dependent loads on the critical components can be controlled. This control action is usually indirectly applied by manipulating performance control inputs. The damage could derive from a variety of mechanisms such as microcracking wear, creep, fatigue, spalling, corrosion, and other mechanisms at one or more critical points. The time derivative of damage $\dot{D}$ indicates how the instantaneous load is affecting the structural components. The plant and remaining system dynamics in figure 2.1 are modeled by nonlinear differential equations which satisfy the local Lipschitz condition (Vidyasagar, 1992) within the domain of the plant operating range. The structural model consists of the solution of structural dynamic equations representing the critical components under load conditions. This model may be a detailed representation of the structural dynamic behavior of critical plant elements or may be as simple as the isolated loads at the critical points determined from minor computations. A general structure of the plant and damage dynamics and their constraints is represented as follows:

Plant Dynamics:

$$\frac{dx(t)}{dt} = f(x(t), u(t)); \quad x(t_0) = x_0 \tag{2.1}$$

Performance Controller:

$$x_p(k+1) = Ax_p(k) + B\left[y_{CMD}(k) - y(k)\right] \tag{2.2a}$$

$$u_p(k) = Cx_p(k) + D\left[y_{CMD}(k) - y(k)\right] \tag{2.2b}$$

Damage Controller:

$$x_d(k+1) = Ex_d(k) + F\dot{D}(k) \tag{2.3a}$$

$$u_d(k) = Gx_d(k) + H\dot{D}(k) \tag{2.3b}$$

Structural Estimator:

$$q = f_1(y) \tag{2.4}$$

Damage Model:

$$\dot{D} = f_2(q) \tag{2.5}$$

3. The Reusable Rocket Engine

This section contains details on the plant used in this study. The plant under control is a reusable bipropellant rocket engine shown schematically in figure 3.1. The propellants, namely, liquid hydrogen fuel and liquid oxygen, are individually pressurized by separate closed-cycle turbopumps. Pressurized cryogenic fuel and oxygen are pumped into two high-pressure preburners which feed the respective turbines with fuel-rich hot gas. The fuel and oxidizer turbopump speeds and, hence, the propellant flow into the

main thrust chamber are controlled by the respective preburner pressures. The exhaust from each turbine is injected into the main combustion chamber where it burns with the remaining oxidizer and is expanded through the rocket nozzle to generate thrust. The oxygen flow into each of the two preburners is independently controlled by the respective servo-controlled valves. The plant outputs of interest are the O_2/H_2 mixture ratio the and main thrust chamber pressure which are closely related to the rocket engine performance in terms of specific impulse, thrust, and combustion temperature.

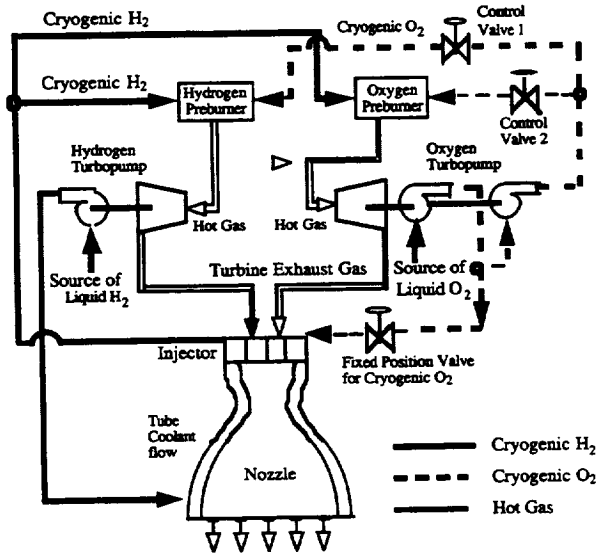

Figure 3.1.- Schematic diagram of reusable bipropellant engine.

A thermo-fluid-dynamic model of the rocket engine has been formulated for plant performance analysis and control systems synthesis (Ray and Dai, 1995). Standard lumped parameter methods have been used to approximate the partial differential equations describing mass, momentum, and energy conservation by a set of first-order differential equations. The plant model is constructed by causal interconnection of the primary subsystem models such as main thrust chamber, preburners, turbopumps, fuel and oxidizer supply header, and fixed nozzle regeneration cooling. In this model, the plant has 18 state variables, two control inputs, and two outputs being controlled. The details of model development are presented in the appendix.

4. Damage Modeling

Damage modeling is a critically important aspect of life extending control. The damage model should have the following characteristics. The model should be continuum based as opposed to cycle based for use in the control design process as well for implementation. Since the model is embedded in the life extending control loop it should be as mathematically, and/or computationally, simple as possible while representing the damage rate well enough to properly guide the actions of the controller. The implication of this is that the absolute level of the damage rate may not be so important as the form of the damage equation (or formulation). Further, computational simplicity becomes especially important when optimization is used in the design process.

A wide variety of damage mechanisms are possible in the reusable rocket engine studied in this report. These include fatigue, spalling, high temperature creep, corrosion, and more. The objective of this report is to establish a viable design method for LEC systems containing extreme nonlinearities. Fatigue damage of the oxygen and hydrogen turbopump turbine blades is selected as the damage mechanism (and critical locations). As will be seen, this type of damage is extremely nonlinear and damage controller synthesis techniques which work for it will likely be adequate for other damage mechanisms.

The fatigue damage model used in this study is a continuum-based analytical model (Lorenzo, 1994). This damage model offers two levels of treatment: (1) a local stress based model and (2) a more accurate strain-strain rate based model. Because of its simplicity and the easy availability of stress estimates, the stress based approach is chosen. For purposes of this study it is assumed that damage only occurs during tensile loading. Three specific damage rate models may be used to estimate damage rate $\dot{D}$.

For the case of zero mean tensile stress

$$\dot{D}(t) = -\frac{2}{b\sigma'_f}\left(\frac{\sigma}{\sigma'_f}\right)^{-(1+b)/b}\frac{d\sigma}{dt} \quad for\ \sigma > 0, \sigma\ \text{increasing} \tag{4.1}$$

where σ is the instantaneous stress, and b and σ'_f are material constants. When the mean stress is not zero, the damage rate is determined as

$$\dot{D}(t) = -\frac{2}{b_f}\left(\frac{1}{\sigma'_f - \sigma_m}\right)^{-1/b}(\sigma - \sigma_m)^{-(1+b)/b}\frac{d\sigma}{dt} \quad for\ \sigma \geq \sigma_m \geq 0,\ \sigma\ \text{increasing} \tag{4.2}$$

where σ_m is the mean stress. Finally, under some conditions, it may be desirable to use a maximum damage rate equation, namely,

$$\dot{D}(t)_{\max} = \frac{2(1+b)^{-(1+b)/b}}{\sigma'_f - \sigma}\frac{d\sigma}{dt} \quad for\ \sigma'_f > \sigma_m \geq 0. \tag{4.3}$$

This form provides an estimate of the instantaneous damage rate which is greater than the damage rate for any mean stress and is a conservative estimate for conditions when the LEC approach is to reduce peak stresses and mean stress is difficult to estimate. For the current application it will be seen that the damage mitigation is derived from reducing the mean stress on the turbine blades. Therefore, the mean stress damage rate equation (eq. (4.2)) is integrated to give the damage increment in one stress cycle as

$$\delta_{cyc} = 2\left(\frac{\sigma_a}{\sigma'_f - \sigma_m}\right)^{-1/b} \tag{4.4}$$

where σ_a is the stress amplitude, σ_m is the mean stress, σ'_f = 223.589 ksi is the fatigue strength coefficient, and b = –0.0858 is the fatigue strength exponent. It is noted that the fatigue strength coefficient was adjusted by a factor of 0.82 to best match a more detailed damage model. The damage rate is calculated from the relation

$$\dot{D} = \left(\frac{\sigma_a}{\sigma'_f - \sigma_m}\right)^{-1/b}\frac{\Omega}{\pi} \tag{4.5}$$

where Ω is the frequency of vibration of the blades in rad/sec. This model is used for both on-line damage estimation and in the optimization (off-line damage estimation).

5. Design of the Dynamic Performance Controller

The design of the inner loop performance controller is not the focus of this study. However, it must yield a well-behaved, stable closed-loop system compatible with the outer loop design process. It is designed to achieve aggressive dynamic response independent of damage considerations. The design procedure employed here uses the H_∞ (or induced L_2 norm to L_2 norm) controller synthesis technique. This controller design method minimizes the worst case gain between the energy of the exogenous inputs and the energy of the regulated outputs of a generalized plant which is constructed below. Bamieh and Pearson (1992) propose a solution to the induced L_2 norm controller synthesis problem for application to sampled-data systems. This design procedure has subsequently been incorporated as the function *sdhfsyn* in the MATLAB *mutools* toolbox (Balas et al., 1993). The performance controller needs to have very good low frequency disturbance rejection capabilities to prevent the damage controller output u^{dam} from causing a long settling time in the plant outputs.

Figure 5.1 shows the setup used for the synthesis of the induced L_2 norm controller for the rocket engine based on a plant model with two inputs (fuel preburner oxidizer valve position and oxidizer preburner oxidizer valve position) and two outputs (main thrust

chamber hot-gas pressure and O_2/H_2 mixture ratio). The plant model is obtained by first linearizing the 18-state nonlinear model of the rocket engine at a combustion pressure of 2550 psi and an O_2/H_2 ratio of 6.02. The bandwidth of the valves is assumed to be nonlimiting for this study. The pressure 2550 psi is chosen for linearization because the controller is required to operate in the range of 2100 to 3000 psi. After linearization, the 18-state linear model is reduced to a 13-state linear model for the controller design via Hankel model order reduction (Zhou, Doyle, and Glover, 1996). A comparison of Bode plots reveals that reducing the 18-state model to 13 states does not significantly alter the input-output characteristics of the original model. Since the induced L_2-norm controller synthesis procedure being used here requires a strictly proper generalized plant model, the problem of a nonzero D-matrix is circumvented by filtering the outputs of the controller by a first order filter with a very high frequency pole at 10^5 rad/sec, that is,

$$W_{filter}(s) = \frac{10^5}{s+10^5}. \tag{5.1}$$

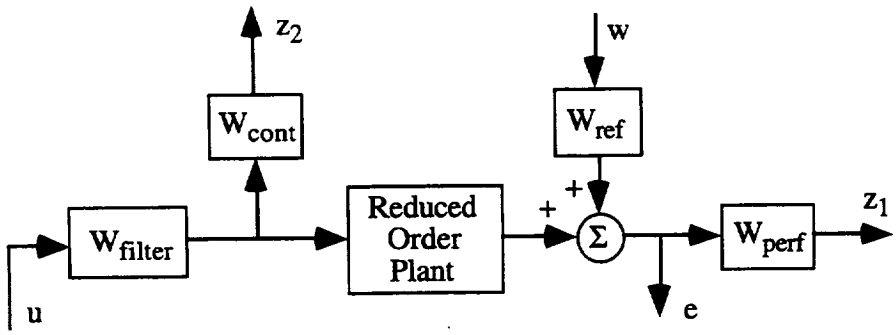

Figure 5.1.—Generalized plant.

The frequency-dependent performance weight W_{perf} consists of two components: (1) W_{press}, which penalizes the tracking error of combustion chamber pressure, and (2) W_{O_2/H_2}, which penalizes the tracking O_2/H_2 error of the O_2/H_2 ratio. The frequency-dependent control signal weight W_{cont} consists of two components: (1) W_{H_2} which penalizes the fuel preburner oxidizer valve position, and (2) W_{O_2} which penalizes the oxidizer preburner oxidizer valve position. The objectives of the performance weights in this application are to keep steady-state error and overshoot/undershoot small while, at the same time, allowing a reasonably fast rise time. The objectives of these control signal weights are (1) prevention of large oscillations in the feedback control signal that may cause valve saturation and (2) reduction of valve wear and tear resulting from high-frequency movements.

The parameters of both performance and control signal weights are initially selected based on the control system performance requirements and the knowledge of the plant dynamics; subsequently, the parameters are fine tuned based on the time-domain responses of the simulation experiments. For this design, the performance weights are

$$W_{press}(s) = 4\left(\frac{s+1.75}{s+1}\right) \tag{5.2}$$

and

$$W_{O_2/H_2}(s) = 4000\left(\frac{s+0.5}{s+0.1}\right). \tag{5.3}$$

The control weight for both valves is

$$W_{H_2}(s) = W_{O_2} = 1200\left(\frac{s+0.75}{s+10}\right). \tag{5.4}$$

Each of the two components of the frequency-dependent reference signal weight W_{ref} in figure 5.1 is chosen to be

$$W_{ref}(s) = \frac{0.5}{s+0.5}. \tag{5.5}$$

A sampled-data controller, which is optimal in the induced L_2-norm sense, is designed using the generalized plant from figure 5.1. As guaranteed by the design method employed, the controller has 21 states, which is the same as the number of states in the generalized plant model which consists of the reduced order plant model (13 states), the control signal filters (2 states), the performance weighting matrix (2 states), the reference signal weighting matrix (2 states), and the control signal weighting matrix (2 states). The controller provides acceptable reference signal tracking for the plant without using a large amount of control effort. It is found that reducing the order of the sampled-data controller from 21 states to 15 states causes no significant change in the controller dynamics from an input/output point of view. Therefore, this reduction causes no noticeable difference in the simulation results produced by the 21- and 15-state controllers. The 15-state controller is used in what follows.

6. Damage Controller Design

This section describes the design of the nonlinear damage-mitigating control loop. Here the output of a linear damage controller is added directly to the input of the plant, as shown in figure 2.1. The plant input is

$$u(k) = u_{ff}(k) + u_{fb}(k) + u_{dam}(k) \tag{6.1}$$

where $u_{ff}(k)$ is a feedforward signal based on linear interpolation of steady-state values of the plant inputs, $u_{fb}(k)$ is the output of the performance controller, and $u_{dam}(k)$ is the output of the damage controller. The damage controller is chosen to be a linear time-invariant discrete time structure. The procedure to be discussed below can be applied to damage controllers with a nonlinear structure; however, for simplicity, the procedure is demonstrated here using a linear damage controller. This section discusses a method which can be used to obtain the state space matrices (i.e., the A, B, C, and D matrices) of the linear damage controller.

The linear damage controller is designed by directly optimizing the elements of its A, B, C, and D matrices. To decrease the number of parameters to be optimized, the A matrix is constrained to be a diagonal matrix with distinct real elements. This is equivalent to constraining the damage controller to having unrepeated real eigenvalues. Repeated and/or complex poles can be included at the expense of computational complexity. For a damage controller with m inputs, p outputs, and n states, the number of parameters to be optimized is n (for the diagonal n×n A matrix) + nm (for the n×m B matrix) + pn (for the p×n C matrix) + pm (for the p×m D matrix) = n(1 + m + p) + pm parameters.

The parameters of the linear dynamic filter are identified by minimizing a cost functional using nonlinear optimization. For each evaluation of the cost functional, a nominal computer simulation must be performed. The cost functional is evaluated by the simulation, and the simulation results are a function of the current damage controller chosen by the optimization routine. Since damage controllers designed using this method are directly based on the maneuver used in the optimization process, the maneuver should be chosen to be broadly representative of all plant operation. The resulting damage controller is then validated by examining the results of various other typical maneuvers that the plant is expected to perform with this damage controller in the damage feedback loop.

The simulation on which the design of the damage controller is based is a ramp-up of the main thrust chamber hot gas pressure from a level of 2700 to 3000 psi at a rate of 3000 psi/sec, followed by a steady state at the final 3000-psi pressure for 500 ms (see fig. 6.1). The O_2/H_2 mixture ratio for this simulation is to be kept at a constant value of 6.02. After each simulation is performed, data representing the results of the simulation are sent to the cost functional subroutine. These data consist of samples at every T = 0.002 sec of the chamber pressure, the O_2/H_2 mixture ratio, the damage rate in the O_2 turbine blade, and the damage rate in the H_2 turbine blade. Since the duration of the simulation is 0.6 sec and each trajectory is sampled every T = 0.002 sec, there is a total of N = 300 samples sent to the cost functional subroutine for each of the four trajectories listed above. In addition, the value of accumulated damage for the O_2 and H_2 turbines at time t = 0.6 sec is also used for the calculation of the value of the cost functional.

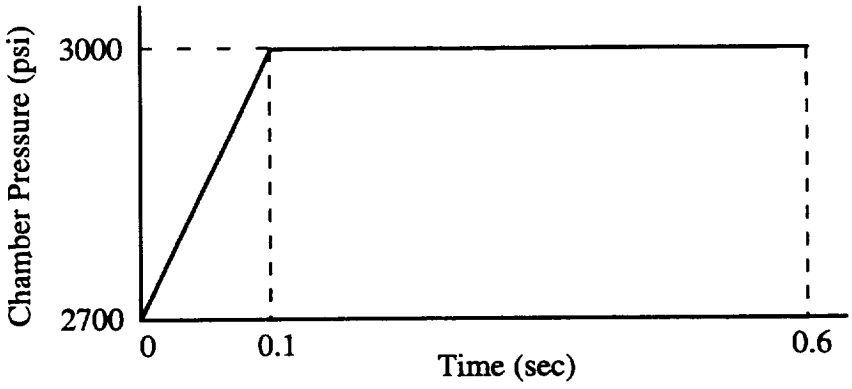

Figure 6.1. - Reference trajectory for chamber pressure.

The cost functional includes the effects of both reference signal tracking (dynamic) performance and damage in the turbine blades; that is,

$$J^{tot} = J^{perf} + J^{dam}. \tag{6.2}$$

The performance part of the cost functional J^{perf} is the sum of penalties on

(1) Tracking error of the main thrust chamber hot gas pressure (in units of psi)

$$J_{press} = \sum_{k=1}^{N-1} Q_{press}\left[\frac{y_{press}(kT) - y_{press}^{ref}(kT)}{y_{press}^{ref}(kT) + 1.0}\right]^2 \tag{6.3}$$

and

$$J_{press}^{ss} = Q_{press}^{ss}\left[\frac{y_{press}(NT) - y_{press}^{ref}(NT)}{y_{press}^{ref}(NT) + 1.0}\right]^2. \tag{6.4}$$

(2) Tracking error of the O_2/H_2 mixture ratio

$$J_{O_2/H_2} = \sum_{k=1}^{N-1} Q_{O_2/H_2}\, g(kT) \tag{6.5}$$

where

$$g(kT) = \begin{cases} \left[\dfrac{y_{O_2/H_2}(kT) - 6.02}{6.02 + 1.0}\right]^2 & \text{if } y_{O_2/H_2}(kT) \geq 6.04 \\ 0 & \text{otherwise} \end{cases} \tag{6.6}$$

and

$$J^{ss}_{O_2/H_2} = Q^{ss}_{O_2/H_2}\left[\frac{y_{O_2/H_2}(NT) - 6.02}{6.02 + 1.0}\right]^2 \tag{6.7}$$

The need for weighting the O_2/H_2 mixture ratio is to prevent thermal excursion damage of the thrust chamber. This occurs as the mixture ratio increases above the nominal set point of 6.02 and is the basis of equation (6.6). The fatigue damage part of the cost functional J^{dam} is composed of penalties on

(1) Damage rate in the O_2 turbine blades

$$J_{\dot{D}_{O_2}} = \sum_{k=1}^{N} Q_{\dot{D}_{O_2}} \dot{D}_{O_2}(kT) \tag{6.8}$$

(2) Damage rate in the H_2 turbine blades

$$J_{\dot{D}_{H_2}} = \sum_{k=1}^{N} Q_{\dot{D}_{H_2}} \dot{D}_{H_2}(kT) \tag{6.9}$$

(3) Accumulated damage in the O_2 turbine blades

$$J_{D_{O_2}} = Q_{D_{O_2}}\left[D_{O_2}(NT) - D_{O_2}(0T)\right] \tag{6.10}$$

(4) Accumulated damage in the H_2 turbine blades

$$J_{D_{H_2}} = Q_{D_{H_2}}\left[D_{H_2}(NT) - D_{H_2}(0T)\right]. \tag{6.11}$$

Both the pressure and O_2/H_2 ratio components of the cost functional have extra weight on the error at the final sampling instant (i.e., the N^{th} sample). Adjusting these extra weights is a means to control the steady-state behavior of the simulation. Increasing Q^{ss}_{press} and/or $Q^{ss}_{O_2/H_2}$ tends to decrease the settling time of the system. Also, since it is desirable to keep the O_2/H_2 mixture ratio below a value of 6.04 during the transient, the O_2/H_2 mixture ratio is penalized only if it exceeds 6.04 for samples 1 to N – 1. The final, N^{th}, sample of the O_2/H_2 ratio is penalized whether its value is above or below 6.04, since it is necessary for the O_2/H_2 ratio to reach 6.02 in the steady state. The factor of 1.0 added in the denominator of equations (6.3), (6.4), (6.6), and (6.7) is a convenient way to combine the features of absolute and relative error and is often used in practice (Gill, Murray, and Wright, 1981).

The accumulated damage and damage rate components of the cost functional do not contain an absolute value operator or squared terms because damage rate and accumulation are always positive. In the accumulated damage components (eqs. (6.10) and (6.11)), the initial accumulated damage is subtracted from the final damage at time NT = 0.6 sec to penalize the damage accumulated during the maneuver. The initial fatigue damage for both the O_2 and the H_2 turbine blades is assumed to be D(0) = 0.1.

Since the governing equations and the cost functional are nonlinear in nature, a nonlinear programming technique is used to identify the optimal parameters of the damage controller. Also, in order to evaluate the cost functional, a time consuming simulation must be performed. Therefore, a nonlinear programming technique known as Sequential Quadratic Programming (SQP) is employed; this technique has the reputation of being able to efficiently and successfully solve a wide range of nonlinear programming problems in which the evaluation of the cost functional is a computationally intensive procedure (Schittkowski, 1985). A Sequential Quadratic Programming (SQP) Fortran Software package developed by Gill et al. (1986) at Stanford University called NPSOL is utilized to design the damage controller.

Interaction effects between the damage controller and the performance controller are minimized (1) by requiring a high level of dynamic performance through the cost functional for the nonlinear optimization of the damage controller, and (2) by the inherent frequency separation of the high frequency damage loop and the lower frequency performance loop.

The following set of weights are found to produce an effective damage controller:

$$Q_{press} = 21.0 \qquad Q_{\dot{D}_{O_2}} = 719.42$$

$$Q^{ss}_{press} = 10.6 \qquad Q_{\dot{D}_{H_2}} = 5.31 \times 10^4$$

$$Q_{O_2/H_2} = 2.6 \times 10^8 \qquad Q_{D_{O_2}} = 3.60 \times 10^5$$

$$Q^{ss}_{O_2/H_2} = 2.6 \times 10^8 \qquad Q_{D_{H_2}} = 2.66 \times 10^7$$

7. Simulation Results and Discussion

The rocket engine is a two-input, two-output application (m = 2, p = 2), and the damage controller is designed using 15 states (n = 15). Therefore, the number of parameters to be optimized is 79. It is found that, after designing the 15-state damage controller, reducing the number of states to 5 via Hankel model order reduction does not significantly change the input/output characteristics of the controller. Therefore, the results that follow are created by using the 5-state reduced order damage controller. This result implies that it would be more efficient to directly optimize a controller with 5 states instead of 15 states. Unfortunately, it is not known *a priori* how to optimally choose the number of controller states.

The damage controller is designed based on a transient which takes the chamber pressure from 2700 to 3000 psi (see figs. 7.1 to 7.6). Each plot displays the following cases: (1) no damage control (i.e., $u(k) = u_{ff}(k) + u_p(k)$) and (2) with damage control (i.e., $u(k) = u_{ff}(k) + u_p(k) + u_d(k)$).

The chamber pressure trajectories for the two cases are compared in figure 7.1. The damage controller causes a slower rise time, a longer settling time, and less overshoot in the chamber pressure transient. The damage controller also causes the O_2/H_2 ratio to deviate farther from the desired value of 6.02 than the case with no damage control as seen in figure 7.2. However, the mixture ratio settles to 6.02 at steady state and remains within acceptable bounds throughout the duration of the simulation for both cases.

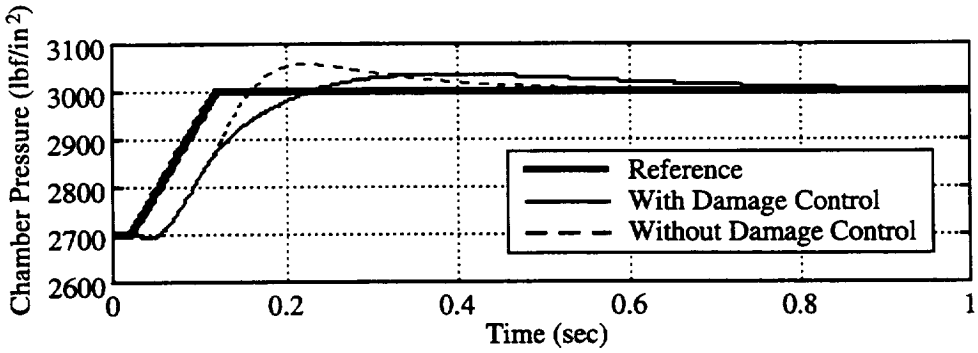

Figure 7.1. - Main combustion chamber hot gas pressure (2700 to 3000 psi).

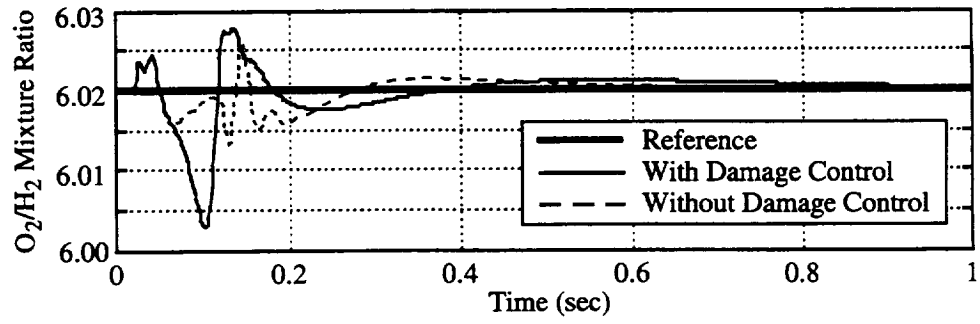

Figure 7.2. - O_2/H_2 mixture ratio (2700 to 3000 psi).

The damage rate and accumulation plots for the first 1 sec of the 2700- to 3000-psi simulation are shown in figures 7.3 to 7.6. Also, Table I summarizes the accumulated damage after this time interval for the two simulation cases (i.e., with and without damage control) for the two turbine blades.

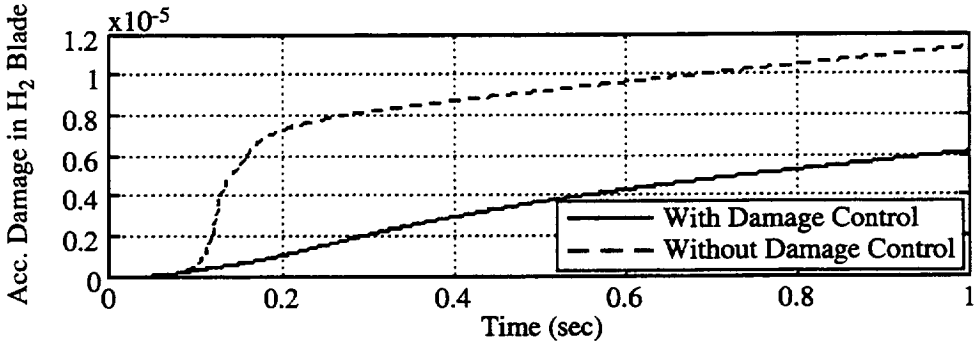

Figure 7.3. - Accumulated damage in H_2 blade (2700 to 3000 psi).

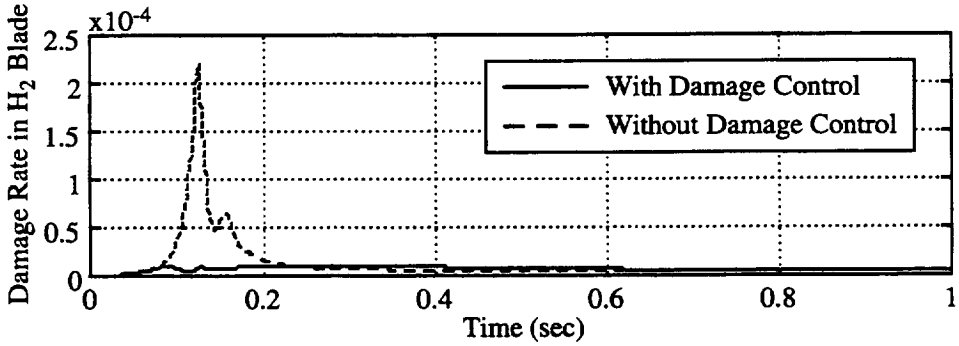

Figure 7.4. - Damage rate in H_2 blade (2700 to 3000 psi).

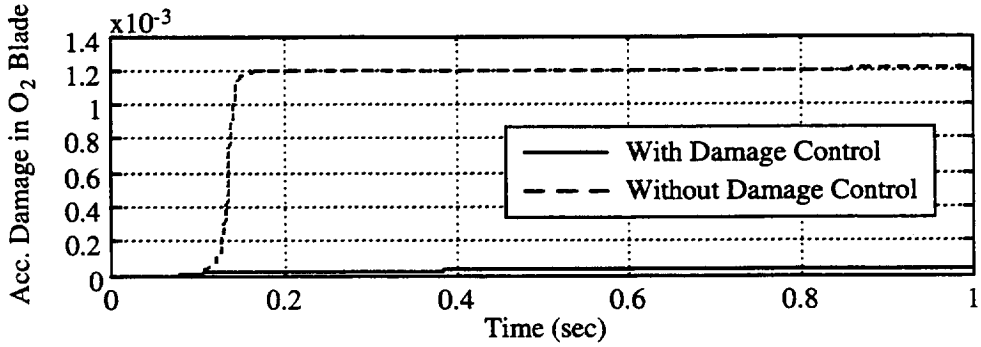

Figure 7.5. - Accumulated damage in O_2 blade (2700 to 3000 psi).

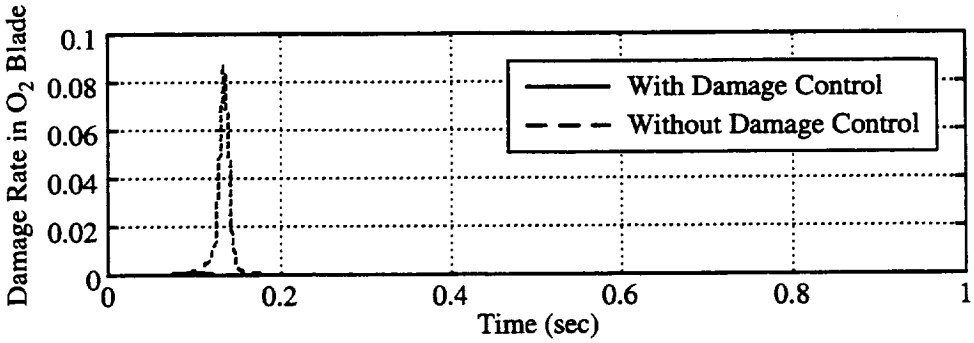

Figure 7.6. - Damage rate in O_2 blade (2700 to 3000 psi).

TABLE I. —ACCUMULATED DAMAGE (AFTER 1 sec) FOR 2700- to 3000-psi SIMULATION

	Without damage control	With damage control	Ratio
H_2 blades	1.13×10^{-5}	6.15×10^{-6}	1.8
O_2 blades	1.21×10^{-3}	3.45×10^{-5}	35.1

The loss of dynamic response of chamber pressure (fig. 7.1) and the modestly increased excursion in mixture ratio is the cost incurred for the improved damage performance. It is also observed that the slope of the accumulated damage (damage rate) at t = 1.0 sec for the H_2 turbine blade (fig. 7.3) indicates that there may be a relatively large steady-state damage rate for that turbine. If this is found to be the case for longer times, then the steady-state damage accumulation would far outweigh the transient damage.

The quality of the damage controller designed above is now tested on a transient maneuver which takes the chamber pressure from 2100 to 3000 psi at a rate of 3000 psi/sec (see figs. 7.7 to 7.12). This maneuver involves a larger pressure increase than the nominal maneuver used to design the damage controller, and, therefore, is expected to produce a larger amount of damage accumulation.

A comparison of the chamber pressure trajectories with and without the damage controller is shown in figure 7.7. As in the 2700- to 3000-psi case, the damage controller acts to "slow down" the transient as it approaches the final pressure of 3000 psi. Although the damage controller causes the O_2/H_2 ratio to deviate from the desired value of 6.02 more than it did during the 2700- to 3000-psi simulation, as seen in figure 7.8, it settles to 6.02 at steady state and remains within acceptable bounds throughout the simulation. The mixture ratio is important in this application as an indicator of chamber temperature (as well as propellant utilization) since the damage model does not contain temperature effects. Future implementations of the damage model can incorporate such effects.

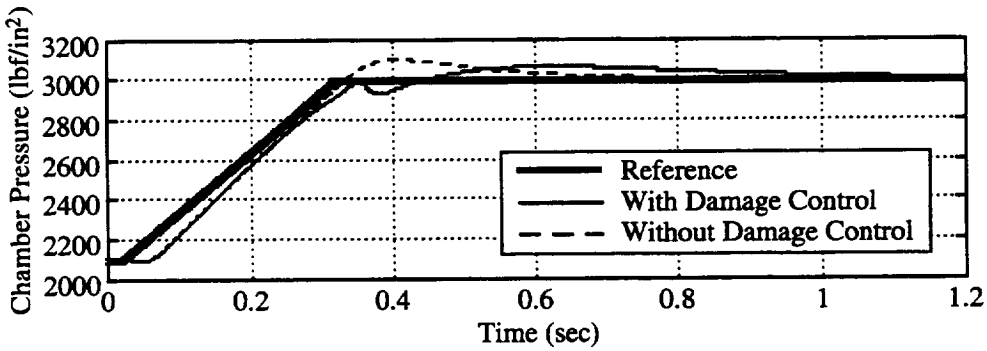

Figure 7.7 - Main combustion chamber hot gas pressure (2100 to 3000 psi).

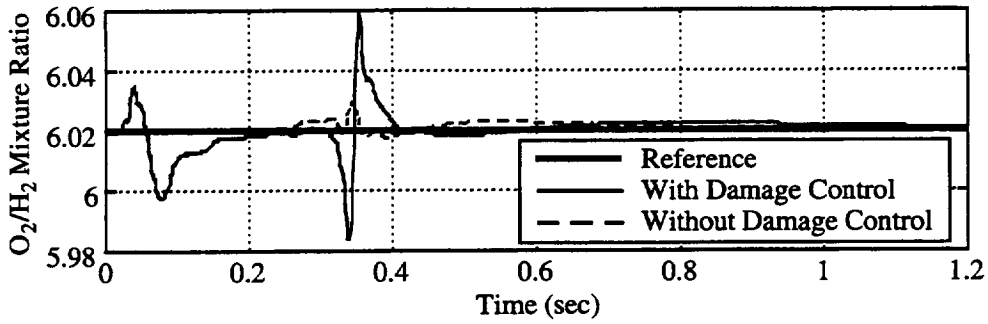

Figure 7.8.- O_2/H_2 mixture ratio (2100 to 3000 psi).

The damage rate and accumulation plots for the first 1.2 sec of the 2100- to 3000-psi simulation are shown in figures 7.9 to 7.12. Table II summarizes the accumulated damage for this transient.

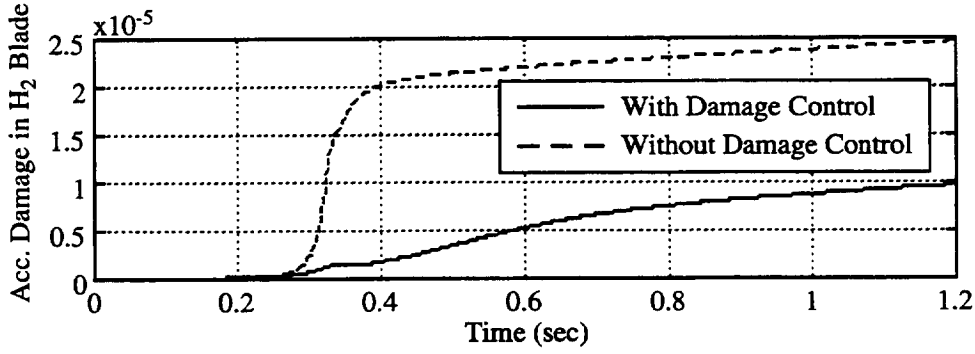

Figure 7.9. - Accumulated damage in H_2 turbine blade (2100 to 3000 psi).

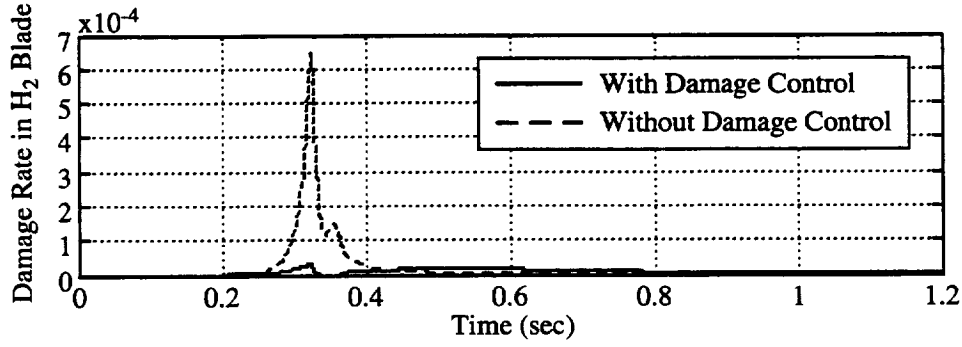

Figure 7.10. - Damage rate in H_2 turbine blade (2100 to 3000 psi).

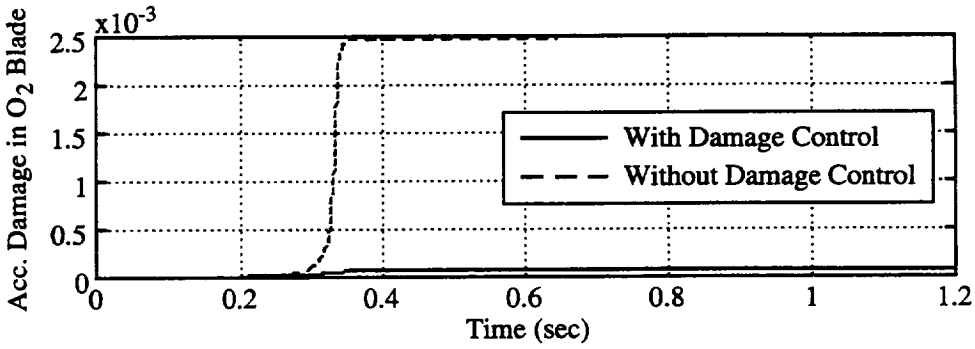

Figure 7.11. - Accumulated damage in O_2 turbine blade (2100 to 3000 psi).

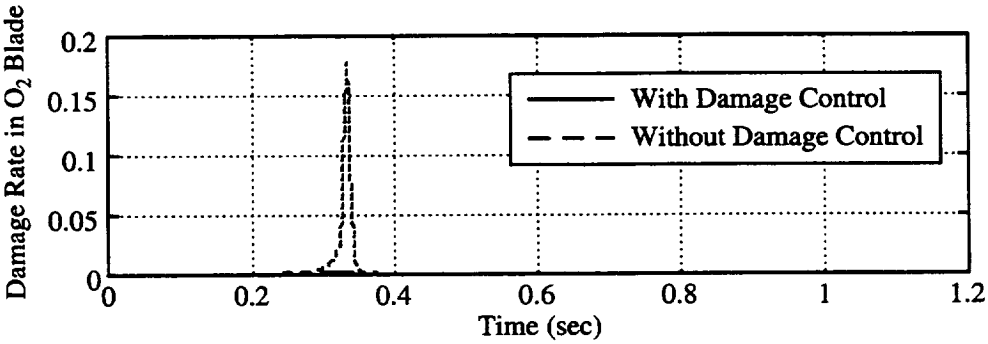

Figure 7.12. Damage rate in O_2 turbine blade (2100 to 3000 psi).

TABLE II.—ACCUMULATED DAMAGE (AFTER 1.2 sec) FOR 2100- to 3000-psi SIMULATION

	Without damage control	With damage control	Ratio
H_2 blades	2.46×10^{-5}	9.61×10^{-6}	2.6
O_2 blades	2.48×10^{-3}	7.01×10^{-5}	35.4

A deeper understanding of how the damage reduction is achieved may be obtained by observing the other state variables. The mechanism for damage reduction in this application is the reduction of mean stress on the turbine blades. This is achieved by the control by reduction of the peak value of turbine torque response (figs. 7.13 and 7.14).

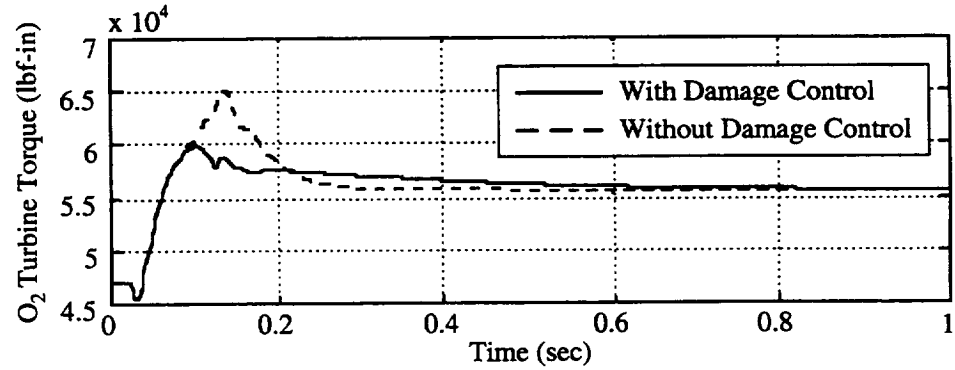

Figure 7.13. - Torque response in O_2 turbine (2700 to 3000 psi).

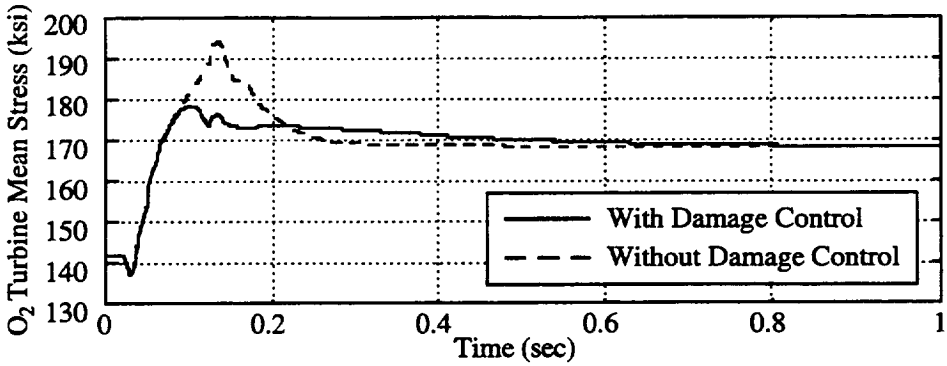

Figure 7.14. - Mean stress in O_2 turbine blade (2700 to 3000 psi).

8. Summary and Conclusions

The key concept of life extending control (LEC), as presented in this report, is to separate the design of the performance controller and the damage controller. A two-tier architecture has been proposed for the life extending control system which consists of a linear performance controller in the inner loop and a nonlinear damage controller in the outer loop. The high performance controller in the inner loop is designed using standard (linear) techniques (H_∞ or μ) to achieve an acceptable dynamic response for a reusable rocket engine which is similar to the Space Shuttle Main Engine (SSME). The combination of the rocket engine dynamics and the performance controller in the inner loop becomes the augmented plant for the design of the nonlinear damage controller (in the outer loop) which is the cascaded combination of a nonlinear characterization of fatigue damage rate in the turbine blades and a linear dynamic filter. The parameters of the filter are optimized to reduce the damage rate and accumulation at the critical points (i.e., fuel and oxidizer turbine blades) specifically under transient operations during which time the time-dependent load on the stressed structure is controllable. Benefits of this controller design approach are the following: (1) the performance controller can be designed by conventional (linear) techniques using commercially available software, (2) the effectiveness of the damage controller can be readily assessed relative to the reference design, and (3) when properly designed, the two-tier controller architecture can function over a broad range of transient requests (inputs) and not require an optimized feed-forward control sequence which is sensitive to plant modeling uncertainties and variations in the initial conditions.

The damage controller designed in Section 6 reduces transient damage in the turbine blades of the reusable rocket engine by factors of 1.8 to 35 times as compared to when there is no damage controller in place. This reduction results in only a very small amount of degradation in the transient performance.

Guaranteeing the stability of the closed-loop system is the single most important requirement of any control system design. For linear time-invariant systems stability can easily be determined by examining the eigenvalues of the A matrix of the closed-loop system. However, in general, proving the stability of nonlinear and/or time-varying systems is not very straightforward. In fact, for some complex systems it can be nearly impossible to analytically establish the stability of the system. Unfortunately, since fatigue damage processes contain severe nonlinearities, control systems containing a damage model in a feedback loop are nonlinear, and possibly time-varying as well. For the control system designed here, typical simulations were performed for which the closed-loop system was stable. Further, the apparent stability was increased as manifested by the chamber pressure response. However, for nonlinear systems, good performance and stability for a set of simulations does not guarantee that the system will be stable for a simulation not in that set. For this reason a rigorous proof of the stability of damage-mitigating control systems should be pursued. Unfortunately, at this time, no proof of the stability of damage-mitigating control systems is available. A formal proof is a subject of future research.

APPENDIX

THERMO-FLUID DYNAMIC MODELING OF THE REUSABLE ROCKET ENGINE*

This chapter (Ray and Dai, 1995) presents a nonlinear dynamic model of the thermal-fluid dynamics in a reusable rocket engine. The purpose of this model is to represent the overall dynamic performance and component interactions with sufficient accuracy for control synthesis and damage prediction. The governing equations used in the model are based on the fundamental principles of physics as well as on the experimental data under a variety of plant operating conditions. The model is formulated in the state-variable setting via nonlinear differential equations with time-invariant coefficients.

The operating principles of the rocket engine under consideration are briefly described in Section A.1. Section A.2 presents the development of the nonlinear dynamic model equations using lumped parameter approximation.

A.1 Description of the Reusable Rocket Engine

The reusable bipropellant rocket engine, under consideration in this report, is similar to the Space Shuttle Main Engine (SSME). Figure 3.1 in the mainbody of the report shows a functional diagram for operations and control of the rocket engine. The propellants, namely, liquid hydrogen and liquid oxygen, are individually pressurized by separate turbopumps. Pressurized liquid hydrogen and oxygen are pumped into individual high-pressure preburners which feed the respective turbines with fuel-rich hot gas. The exhaust gas from each turbine is mixed in the common manifold and then injected into the main combustion chamber where it burns with the oxidizer to make most efficient use of the energy liberated by combustion. The oxygen flow into each of the two preburners is independently controlled by the respective servo-valve while the valve position for oxygen flow into the main thrust chamber is held in a fixed position to derive maximum possible power from the engine. The plant outputs of interest are O_2/H_2 mixture ratio and combustor pressure which are closely related to the rocket engine performance in terms of thrust-to-weight ratio and engine efficiency. The liquid hydrogen is used as a regenerative coolant for the walls of the combustion chamber and thrust nozzle where structural integrity is endangered by the high temperature environment. The pressurized liquid fuel is circulated through the coolant jackets to absorb the heat transferred from the hot reaction gases to the thrust chamber and nozzle walls.

A.2 Development of Plant Model Equations

Standard lumped parameter approaches have been used to model the thermo-fluid dynamics of the engine in order to approximate the partial differential equations describing mass, momentum, and energy conservation by a set of first-order differential equations with time as the independent variable. The plant model is constructed via causal interconnection of the primary subsystem models such as the main thrust chamber, preburners, turbopumps, valves, fuel and oxidizer supply headers, and regenerative cooling systems. The governing equations for the lumped parameter model of the plant dynamics are described in the following sections. In addition to the basic assumption of the lumped parameter approach, other pertinent assumptions are stated while describing the models of the individual subsystems.

A.A.1 Fuel and Oxidizer Turbopump Subsystems

The rocket engine has two sets of turbopumps, namely, low pressure and high pressure, for each of the two propellants. A simplified representation of the dynamic characteristics of the rocket engine is developed by lumping the low pressure and high pressure turbopumps into a single subsystem for each of the fuel and oxidizer propellants. On the oxidizer side, however, two pumps are modeled to obtain two sources of oxygen at different pressures. Model equations for the fuel and oxidizer turbopumps are given in Table A.1 and Table A.2, respectively.

Models of the hydraulic pump subsystems are derived based on the following assumptions:

(a) The pump head which is proportional to the difference between static pressures at the suction and discharge is derived based on the assumptions of: (i) one-dimensional steady incompressible flow with negligible heat transfer; (ii) identical fluid velocities at the suction and discharge section of the pump; and (iii) no change in potential energy

Table A.1.—The fuel turbopump model equations

Fuel Pump Model Equations	Fuel Turbine Model Equations
$S_{PMP} = \int_0^t \dot{S}_{PMP}(t)dt + S_{PMP}(0)$	$T_{PBR} = \frac{P_{PBR}}{R_{PBR} R C_{TBU}} = T_{TRBI}$
$\dot{S}_{PMP} = (X_{TRB} - X_{PMP}) / C_{PMPMI}$	$H_{TRBI} = C_{P,PBR} T_{TRBI}$
$W_{PMP} = (1 + C_{PMPW})(W_{HPBH} + W_{OPBH})$	$G_{TRBP} = \frac{P_{TRBE}}{P_{TRBI}} = \frac{P_{FINJ}}{P_{PBR}}$
$G_{PMP} = C_{PMPG} W_{PMP} / S_{PMP}$	$T_{TRBE,ideal} = C_{TRBTI} T_{TRBI} \times (G_{TRBP})^{k-1/k}$
$G_{PMPP} = \Phi_{PMPP}(G_{PMP})$	$W_{TRB} = C_{TRBW3} \frac{P_{TRBI}}{\sqrt{T_{TRBI}}}$
$G_{PMPD} = C_{PMPP} S_{PMP}^2 G_{PMPP}$	$G_{TRBH} = \sqrt{C_{P,TRB}(T_{TRBI} - T_{TRBE,ideal})}$
$P_{PMPE} = P_{PMPS} + G_{PMPD}$	$G_{TRBX} = C_{TRBX5} \frac{S_{PMP}}{G_{TRBH}}$
$V_{PMP} = W_{PMP} G_{PMPD} / R_{PMPI}$	$X_{TRB} = C_{TRBX5} W_{TRB} G_{TRBH} \times \Phi_{TRBX}(G_{TRBX})$
$X_{PMP} = V_{PMP} / S_{PMP}$	$V_{TRB} = X_{TRB} S_{PMP}$
$G_{PMPE} = (\frac{W_{PMP}}{S_{PMP}}) / (\frac{W_{PMPR}}{S_{PMPR}})$	$G_{TRBE} = (\frac{S_{PMP}}{G_{TRBH}}) / (\frac{S_{PMPR}}{G_{TRBHR}})$
$E_{PMP} = E_{PMPR} \Phi_{PMPE}(G_{PMPE})$	$E_{TRB} = E_{TRBR} \Phi_{TRBE}(G_{TRBE})$
$H_{PMPE} = C_{P,H_2} T_{PMPS} + \frac{V_{PMP}}{W_{PMP}} (\frac{1}{\eta_{PMP}} - 1)$	$H_{TRBE} = H_{TRBI} - G_{TRBH}^2 E_{TRB}$
$T_{PMPE} = H_{PMPE} / C_{P,H_2}$	$T_{TRBE} = H_{TRBE} / C_{P,TRB}$

Table A.2.—The oxidizer turbopump model equations

Oxidizer Pump2 Model Equations	Oxidizer Pump3 Model Equations
$W_{WO} = (1 + C_{OTRIW}) \times (W_{CMBO} + W_{HPBO} + W_{OPBO})$	$W_{OP3} = (W_{HPBO} + W_{OPBO})$
$G_{OP2} = C_{OP2G} W_{WO} / S_{OPMP}$	$G_{OP3} = C_{OP3G} W_{OP3} / S_{OPMP}$
$G_{OP2P} = \Phi_{OPMPP}(G_{OP2})$	$G_{OP3P} = \Phi_{OPMPP}(G_{OP3})$
$G_{OP2D} = C_{OP2P} S_{OPMP}^2 G_{OP2P}$	$G_{OP3D} = C_{OP3P} S_{OPMP}^2 G_{OP3P}$
$P_{OP2PE} = P_{OPMPS} + G_{OP2D}$	$P_{OP3PE} = P_{OPMPS} + G_{OP3D}$
$G_{OP2X} = \Phi_{OP2X}(G_{OP2})$	$G_{OP3X} = \Phi_{OP3X}(G_{OP3})$
$X_{OP2} = C_{OP2X} S_{OPMP}^2 G_{OP2X}$	$X_{OP3} = C_{OP3X} S_{OPMP}^2 G_{OP3X}$
$V_{OP2} = X_{OP2} S_{OPMP}$	$V_{OP3} = X_{OP3} S_{OPMP}$
$G_{OP2E} = \left(\frac{W_{WO}}{S_{OPMP}}\right) / \left(\frac{W_{WOR}}{S_{OPMPR}}\right)$	$G_{OP3E} = \left(\frac{W_{OPP3}}{S_{OPMP}}\right) / \left(\frac{W_{OP3R}}{S_{OPMPR}}\right)$
$E_{OP2} = E_{OP2R} \Phi_{OP2E}(G_{OP2E})$	$E_{OP3} = E_{OP3R} \Phi_{OP3E}(G_{OP3E})$
$H_{OP2E} = C_{P,O_2} T_{OPMPS} + \frac{V_{OP2}}{W_{WO}}\left(\frac{1}{\eta_{OP2}} - 1\right)$	$H_{OP3E} = C_{P,O_2} T_{OP2E} + \frac{V_{OP3}}{W_{OP3}}\left(\frac{1}{\eta_{OP3}} - 1\right)$
$T_{OP2E} = H_{OP2E} / C_{P,O_2}$	$T_{OP3E} = H_{OP3E} / C_{P,O_2}$

Oxygen Turbine Model Equation	
$S_{OPMP} = \int_0^t \dot{S}_{OPMP}(t)dt + S_{OPMP}(0)$	$G_{OTRH} = \sqrt{C_{P,OTR}(T_{OTRI} - T_{OTRE,ideal})}$
$\dot{S}_{OPMP} = (X_{OTR} - X_{OP2} - X_{OP3}) / C_{OPMPI}$	$G_{TRBX} = C_{TRBX4} \frac{S_{OPMP}}{G_{OTRH}}$
$T_{OPB} = \frac{P_{OPB}}{R_{OPB} R C_{TBU}} = T_{OTRI}$	$X_{TRB} = C_{TRBX3} W_{OTR} G_{OTRH} \times \Phi_{OTRX}(G_{OTRX})$
$H_{OTRI} = C_{P,OPB} T_{OTRI}$	$V_{TRB} = X_{TRB} S_{PMP}$
$G_{OTRP} = \frac{P_{OTRE}}{P_{OTRI}} = \frac{P_{FINJ}}{P_{OPB}}$	$G_{OTRE} = \left(\frac{S_{OPMP}}{G_{OTRH}}\right) / \left(\frac{S_{OPMPR}}{G_{OTRHR}}\right)$
$T_{OTRE,ideal} = C_{OTRTI} T_{OTRI} G_{OTRP}^{k-1/k}$	$E_{OTR} = E_{OTRR} \Phi_{OTRE}(G_{OTRE})$
$W_{OTR} = C_{OTRW3} \frac{P_{OTRI}}{\sqrt{T_{OTRI}}}$	$H_{OTRE} = H_{OTRI} - G_{OTRH}^2 E_{OTR}$
	$T_{OTRE} = H_{OTRE} / C_{P,OTR}$

(b) The static performance of the pump is based on empirical characteristics (Rockwell, 1989) where the pump head ΔP_{PMP}, power V_{PMP}, and efficiency η_{PMP} are modeled as functions of the ratio of mass flow rate, W_{PMP}, to pump speed S:

$$\Delta P_{PMP} \propto S^2\Phi_1(\Theta); \quad V_{PMP} \propto S^2\Phi_2(\Theta); \quad \text{and} \quad \eta_{PMP} \propto S\Phi_3(\Theta) \tag{A.1}$$

where $\Theta = W_{PMP}/S$, and the functions Φ_1, Φ_2, and Φ_3 are obtained from Rockwell (1989). Therefore, the outputs of the pump model, namely, pump discharge pressure, temperature, enthalpy, and torque, can be obtained from the pump characteristics and thermodynamic state relations.

The governing equations for the turbine model are formulated under the following assumptions:

(c) The working fluid in the turbine is a perfect gas and the expansion process in the turbine is adiabatic. For the ideal frictionless process, the following relationship holds:

$$T_{in}/T_{out,ideal} = \left(P_{in}/P_{out}\right)^{(k-1)/k} \tag{A.2}$$

where T is the absolute temperature, P is the pressure, the subscripts "in" and "out" respectively indicate the inlet and the outlet of the turbine, the subscript "ideal" stands for the idealized isentropic condition, and k is the ratio of the specific heats at constant pressure and temperature, which is assumed to be a constant within the operating range of turbine.

(d) No loss of pressure and enthalpy occurs between the preburner outlet and turbine inlet. That is,

$$P_{PBR} = P_{TRB,in}; \quad \text{and} \quad H_{PBR} = H_{TRB,in} \tag{A.3}$$

(e) Flow through the turbine is assumed to be choked, and the kinetic energy of the fluid in the preburner chamber is negligible such that the stagnation pressure and temperature, P* and T*, are respectively identical to the static preburner pressure and temperature, P and T. Therefore, the mass flow rate W_{TRB} through the turbine can be expressed as:

$$W_{TRB} = C\frac{P^*_{TRB,in}}{\sqrt{T^*_{TRB,in}}} = C\frac{P^*_{PBR}}{\sqrt{T^*_{PBR}}} = C\frac{P_{PBR}}{\sqrt{T_{PBR}}} \tag{A.4}$$

where the coefficient C is calculated from the steady-state data.

(f) The turbine efficiency and the output torque are obtained from the empirical characteristics of the turbine (Rockwell, 1989) as:

$$\eta_{TRB} = \eta^*_{TRB}\Phi\left(\frac{S}{\sqrt{\Delta H_{ideal}}}\right) \tag{A.5a}$$

$$X_{TRB} = W_{TRB}\sqrt{\Delta H_{ideal}}\,\Phi\left(\frac{S}{\sqrt{\Delta H_{ideal}}}\right) \tag{A.5b}$$

where ideal (i.e., isentropic) enthalpy drop ΔH_{ideal} is given as:

$$\Delta H_{ideal} = C_p T_{in}\left(1 - \frac{T_{out,ideal}}{T_{in}}\right) = C_p T_{in}\left[1 - \left(\frac{P_{out,ideal}}{P_{in}}\right)^{\frac{k-1}{k}}\right] \tag{A.6}$$

The outputs of the fuel and oxidizer turbine models, namely, turbine pressure, temperature, enthalpy, flow rate, and output torque are obtained from thermodynamic relations as delineated in Tables A.1 and A.2, respectively.

The state variables in the fuel and oxidizer turbopump subsystems are respectively the shaft speeds S_{PMP} and S_{OPMP}. The power delivered by each turbine is equal to the sum of the power required by the propellant pump, and power losses in the bearings, gears, seals, and wear rings. Therefore, the dynamics of shaft speed in each turbopump are given in terms of the difference in torque as:

$$I\frac{dS}{dt} = \left(X_{TRB} - X_{PMP}\right) \tag{A.7}$$

where I is the moment of inertia and X indicates the torque.

A.A.2 Preburner Fuel and Oxidizer Supply Header Subsystems

The model equations of the preburner fuel and oxidizer supply header subsystems are listed in Table A.3. The equations of fuel flow to each preburner are approximated to simplify the complexity of flow boundaries. The fuel flow to the two preburners accounts for the mixture of the coolant flow from the primary nozzle cooling region and the primary nozzle bypass. The governing equations of the fuel flow through the preburner header are derived under the following assumptions:

(a) The preburner fuel supply pressure P_{FPS} is proportional to the fuel flow pressure at the main fuel valve.

(b) Two coolant flows, namely, main chamber coolant flow (W_{CMBF}) and primary nozzle coolant flow (W_{NOZF}), varies in proportion to the total fuel flow (W_{PMP}). Since the coolant control valve position is held fixed, it is treated as fully open. Accordingly, the fixed nozzle bypass flow is obtained by subtracting the main chamber coolant flow and the nozzle coolant flow as:

$$W_{CMBF} = C_{CMBF}W_{PMP} \tag{A.8a}$$

$$W_{NOZF} = C_{NOZF}W_{PMP} \tag{A.8b}$$

$$W_{FNBP} = W_{PMP} - W_{CMBF} - W_{NOZF} \tag{A.8c}$$

By neglecting the dynamics due to fluid inertance in the flow passages, the above simplifications (a) and (b) reduce four differential equations of momentum conservation into four algebraic equations. This approximation only affects the model accuracy at high frequencies because of relatively small fluid inertance.

(c) For one dimensional, incompressible uniform flow through a pipeline or valve and neglecting the body force, the friction pressure drop through a pipeline or valve is expressed as:

$$\Delta P = f\frac{L}{D}\frac{\rho}{2}\frac{Q^2}{A^2} = C\frac{|W|W}{\rho}, \quad C = f\frac{L}{D}\frac{1}{2A^2}, \quad \text{for pipeline} \tag{A.9a}$$

$$\Delta P = f\frac{L}{D}\frac{\rho}{2}\frac{Q^2}{A^2} = C'\frac{|W|W}{{R_A}^2}, \quad C' = f\frac{L}{D}\frac{1}{2\rho\bar{A}^2}, \; R_A = \frac{A}{\bar{A}} \quad \text{for valve} \tag{A.9b}$$

The state variables of the preburner fuel and oxidizer supply headers are:

- W_{HPBH} and W_{HPBO} (fuel mass flow rates into the fuel and oxidizer preburners);
- W_{OPBH} and W_{OPBO} (oxidizer mass flow rates into the fuel and oxidizer preburners).

The derivatives of the above four state variables are obtained from conservation of linear momentum over a control volume of a pipeline,

$$\frac{d}{dt}(W) = C_f\left(P_{in} - P_{out} - C\frac{|W|W}{\rho}\right), \tag{A.10}$$

where ρ is the average fluid density and C_f is the inverse of equivalent fluid inertance.

Table A.3.—Preburner fuel supply header model equations

Preburner Fuel Supply Header Model Equations	Preburner Oxidizer Supply Header Model Equations
$W_{HPBH} = \int_0^t \dot{W}_{HPBH}(t)dt + W_{HPBH}(0)$	$W_{HPBO} = \int_0^t \dot{W}_{HPBO}(t)dt + W_{HPBO}(0)$
$W_{OPBH} = \int_0^t \dot{W}_{OPBH}(t)dt + W_{OPBH}(0)$	$W_{OPBO} = \int_0^t \dot{W}_{OPBO}(t)dt + W_{OPBO}(0)$
	$W_{CMBO} = \int_0^t \dot{W}_{CMBO}(t)dt + W_{CMBO}(0)$
$P_{MFVD} = P_{PMPE} - C_{PMPFV}\lvert W_{PMP}\rvert W_{PMP}$	$A_{RFPV} = C_{FPVAR} A_{FPV}$
$P_{FPS} = C_{PFPS} P_{MFVD}$	$A_{ROPV} = C_{OPVAR} A_{OPV}$
$W_{CMBF} = C_{CMBF} W_{PMP}$	$A_{RMOV} = 1.0$
$W_{NOFF} = C_{NOFF} W_{PMP}$	$\dot{W}_{HPBO} = C_{HOW0}(P_{OP3PE} - P_{PBR} - C_{HOW1}\lvert W_{HPBO}\rvert W_{HPBO} - C_{HOW2}\frac{\lvert W_{HPBO}\rvert W_{HPBO}}{A_{RFPV}^2})$
$W_{FNBP} = W_{PMP} - W_{CMBF} - W_{NOZF}$	
$H_{NOZFE} = C_{P,H_2} T_{NOZF}$	
$H_{FPS} = (W_{NOZF} H_{NOZFE} + W_{FNBP} H_{PMPE}) / (W_{HPBH} + W_{OPBH})$	$\dot{W}_{OPBO} = C_{OOW0}(P_{OP3PE} - P_{OPB} - C_{OOW1}\lvert W_{OPBO}\rvert W_{OPBO} - C_{OOW2}\frac{\lvert W_{OPBO}\rvert W_{OPBO}}{A_{ROPV}^2})$
$\dot{W}_{HPBH} = C_{HHW0}(P_{PFS} - P_{PBR} - C_{HHW1}\frac{\lvert W_{HPBH}\rvert W_{HPBH}}{R_{PFS}})$	
$\dot{W}_{OPBH} = C_{OHW0}(P_{PFS} - P_{OPB} - C_{OHW1}\frac{\lvert W_{OPBH}\rvert W_{OPBH}}{R_{PFS}})$	$\dot{W}_{CMBO} = C_{CMBW0}(P_{OP2PE} - P_{CMB} - C_{CMBW1}\lvert W_{HPBO}\rvert W_{HPBO} - C_{CMBW2}\frac{\lvert W_{HPBO}\rvert W_{HPBO}}{A_{RMOV}^2})$

A.A.3 Main Chamber Fuel Injector Subsystem

The fuel injector mixes the two branches of fuel-rich exhaust hot-gas from the two turbines and a small amount of fuel from the combustion chamber coolant path. Model equations for the preburners, main thrust chamber, and fuel injector are listed in Table A.4. The governing equations of the fuel injector subsystem are derived under the following assumptions:

(a) The flow of an incompressible working fluid at a low Mach number (e.g., M< 0.3) is governed by the following relation (Blackburn et al., 1960) by assuming that the subsonic velocities exist throughout the orifices:

$$Q = \upsilon A = C_d' A\sqrt{2(P_{in} - P_{out})/\bar{\rho}} \quad \text{(volumetric flow rate)} \tag{A.12a}$$

$$W = Q\rho = C_d\sqrt{2(P_{in} - P_{out})/\bar{\rho}} \quad \text{(mass flow rate)} \tag{A.12b}$$

where $\bar{\rho}$ is the average density which is approximated as the gas density ρ_{CMB} at the combustor.

(b) The flow into the fuel injector manifold is the sum of two turbine exhaust flows, W_{TRB} and W_{OTR}, and main combustion chamber coolant flow W_{CMBF}. The manifold pressure P_{FINJ} is derived from Eq. (A.12b) as:

$$P_{FINJ} = \frac{(W_{TRB} + W_{OTR} + W_{CMBF})^2}{C_d^2\rho_{CMB}} + P_{CMB} \tag{A.13}$$

(c) The mixed gas temperature at the fuel injector manifold is obtained as a weighted average of the two turbine inlet temperatures, T_{PBR} and T_{OPB}, and the main chamber coolant flow temperature, T_{CMBF}. That is, $T_{FINJ} = C_0T_{PBR} + C_1T_{OPB} + C_2T_{CMBF}$ where the coefficients, C_d, C_0, C_1, and C_2 are obtained from the steady-state data under normal operating conditions.

A.A.4 Oxygen Control Valve Subsystem

The nonlinearities of control valves are compensated by inducing the inverse characteristics of valves (Rockwell, 1989) in the control signal such the valve command becomes proportional to the valve area under steady-state operations. The oxygen control valve subsystem model has two state variables, namely, fuel and oxidizer preburner valve rotary positions. The dynamics of each valve are represented by a first order lag as:

$$\frac{d}{dt}(A_{RFPV}) = \frac{A_{REPV} - U_{FPV}}{\tau_{FPV}} \tag{A.15a}$$

$$\frac{d}{dt}(A_{ROPV}) = \frac{A_{ROPV} - U_{OPV}}{\tau_{OPV}} \tag{A.15b}$$

where U_{FPV} and U_{OPV} are the commands to the oxygen control valves, and A_{RFPV} and A_{ROPV} are the effective areas of the oxidizer control valves, and τ is the time constant of the respective valve.

In solving the nonlinear optimal open loop control problem, the two commands U_{FPV} and U_{OPV} correspond to the decision variables in the nonlinear programming which are bounded above and below via specified constraints.

A.A.5 Preburner and Combustion Subsystems

The dynamic equations for the combustion process are developed by employing the principles of conservation of mass and energy with the following assumptions.

(a) Conservation of momentum is satisfied by assuming that gas pressure and temperature in the combustion chamber are spatially uniform although they are time-dependent, and the kinetic energy due to gas velocity in the chamber is negligible. This assumption is valid for a low-frequency dynamic representation, and precludes the process of high-frequency acoustic propagation.

Table A.4.—Valve, preburner, combustion, and fixed nozzle model equations

Oxygen Control Valve Model Equations

$$A_{FPV} = \int_0^t \dot{A}_{FPV}(t)dt + A_{FPV}(0)$$

$$A_{OPV} = \int_0^t \dot{A}_{OPV}(t)dt + A_{OPV}(0)$$

$$\dot{A}_{FPV} = (U_{AFPV} - A_{FPV}) / C_{FPVA}$$

$$\dot{A}_{OPV} = (U_{AOPV} - A_{OPV}) / C_{OPVA}$$

Fuel Preburner Model Equations

$$R_{PBR} = \int_0^t \dot{R}_{PBR}(t)dt + R_{PBR}(0)$$

$$P_{PBR} = \int_0^t \dot{P}_{PBR}(t)dt + P_{PBR}(0)$$

$$\dot{R}_{PBR} = (W_{HPBH} + W_{HPBO} - W_{TRB}) / C_{PBRV}$$

$$\dot{P}_{PBR} = (W_{HPBH} H_{MIX} + W_{HPBO} H_{OP3E} - W_{TRB} H_{TRBI} + W_{HPBO} C_{PBRF}) / C_{PBRL}$$

Oxidizer Preburner Model Equations

$$R_{OPB} = \int_0^t \dot{R}_{OPB}(t)dt + R_{OPB}(0)$$

$$P_{OPB} = \int_0^t \dot{P}_{OPB}(t)dt + P_{OPB}(0)$$

$$\dot{R}_{OPB} = (W_{OPBH} + W_{OPBO} - W_{TRB}) / C_{OPBV}$$

$$\dot{P}_{OPB} = (W_{OPBH} H_{MIX} + W_{OPBO} H_{OP3E} - W_{OTR} H_{OTRI} + W_{OPBO} C_{OPBF}) / C_{OPBL}$$

Main Combustion Model Equations

$$R_{CMB} = \int_0^t \dot{R}_{CMB}(t)dt + R_{CMB}(0)$$

$$P_{CMB} = \int_0^t \dot{P}_{CMB}(t)dt + P_{CMB}(0)$$

$$T_{CMB} = \frac{P_{CMB}}{R_{CMB} CR_{CMB} C_{TBU}}$$

$$H_{CMB} = C_{P,CMB} T_{CMB}$$

$$MR = \frac{W_{CMBO} + W_{OP3}}{W_{PMP}}$$

$$\dot{R}_{CMB} = (W_{FINJ} + W_{CMBO} - W_{NOZ}) / C_{CMBV}$$

$$\dot{P}_{CMB} = (W_{FINJ} H_{FINJ} + W_{CMBO} H_{OP2E} - W_{NOZ} H_{CMB} - Q_{CMBW} + W_{CMBO} C_{CMBF}) / C_{CMBL}$$

Fuel Injector Model Equations

$$P_{FINJ} = (W_{TRB} + W_{OTR} + W_{CMBF})^2 / \left(C_d^2 \rho_{CMB}\right) + P_{CMB}$$

$$T_{FINJ} = C_0 T_{PBR} + C_1 T_{OPB} + C_2 T_{CMBF}$$

$$H_{FINJ} = C_{P,TRB} T_{FINJ}$$

$$W_{FINJ} = C_{FINJW} \frac{P_{FINJ}}{\sqrt{T_{FINJ}}}$$

Fixed Nozzle Model Equations

$$W_{NOZ} = C_{NOZW} \frac{P_{CMB}}{\sqrt{T_{CMB}}}$$

$$C_{MACH} = 1.1$$

$$T_{NOZ} = \frac{T_{CMB}}{[1 + \left(\frac{K-1}{2}\right) C_{MACH}^{\ 2}]}$$

(b) One-dimensional unsteady flow in the combustion chamber is represented by a first order differential equation of the rate change of mixture gas density which is related to the mass flow into and out of the chamber via conservation of mass.

$$\frac{d}{dt}(\rho) = \frac{W_{in} - W_{out}}{V_{CMB}} \tag{A.16}$$

where V_{CMB} is the volume of the combustion chamber.

(c) The conservation of energy equation yields:

$$\frac{d}{dt}(C_V V \rho T) = \sum W_{in} H_{in} - \sum W_{out} H_{out} + F W_{O_2} - Q_{heat} \tag{A.17}$$

where F is the energy liberated by per unit mass of oxygen from a macroscopic point of view of the chemical process where the reaction dynamics is assumed to be instantaneous. Q_{heat} is the heat transfer rate from the control volume to the coolant channel wall.

(d) Based on the thermodynamic relationship of the perfect gas law, the average gas temperature in the combustion chamber is given as: $T_{CMB} = P_{CMB}/(\rho_{CMB} R)$ where R is the characteristic gas constant. Therefore, the derivative of the main chamber pressure is obtained by rewriting the energy Eq. (A.17) as:

$$\frac{d}{dt}(P_{CMB}) = (W_{FINJ} H_{FINJ} + W_{CMBO} H_{OP2E} - W_{NOZ} H_{CMB} + W_{CMBO} F - Q_{CMBW})/(C_V V_{CMB}/R) \tag{A.18}$$

(e) The flow through the nozzle throat is choked.

The model equations of the preburner and combustor are given in Table A.4. The six state variables in two preburners and main combustion chamber are:

- P_{PBR} and R_{PBR}: (Fuel preburner chamber gas pressure and density);
- P_{OPB} and R_{OPB}: (Oxidizer preburner chamber gas pressure and density);
- P_{CMB} and R_{CMB}: (Main thrust chamber hot gas pressure and density).

The governing equations in preburners are similar to those in the main chamber because of the similarity of the physical processes.

A.A.6 Main Thrust Chamber/Fixed Nozzle Cooling Subsystems

The basic relations governing the thrust chamber performance, such as specific impulse, combustion temperature and pressure, are calculated based on the thermodynamic principles of ideal rocket propulsion systems (Sutton, 1992). The following assumptions are used to derive the governing equations of heat transfer in the coolant channel wall.

(a) The hot-gas velocity, pressure, temperature, and density are uniform across any cross-section normal to the nozzle axis.

(b) No shock waves or discontinuities exist in the flow through the convergent-divergent nozzle, and the boundary layer effects are neglected. The energy equation applied across the nozzle throat and nozzle exit yields the exit temperature T_e as a function of the throat temperature, T_t, and exit Mach number M.

$$T_e = \left(\frac{1}{1 + \frac{k-1}{2} M^2} \right) T_t \tag{A.19}$$

where the exit Mach number M can be obtained as a function of the throat/exit pressure ratio, P_t/P_e, and throat/exit area ratio, A_t/A_e, by combining the energy and continuity equations:

$$M = \frac{1}{k-1} \left(-1 + \sqrt{(k-1)(k+1) \left(\frac{A_t}{A_e} \frac{P_t}{P_e} \right)^2 + 1} \right) \tag{A.20}$$

In the simplified model of the main thrust chamber coolant channel subsystem, heat transfer rates and wall temperatures are derived using a lumped parameter model with two nodes. The model equations of the main chamber and nozzle regeneration cooling heat transfer subsystems are listed in Table A.5. The heat transfer process is characterized by three different mechanisms, namely, convective heat flux from the hot gas to hot-side of the coolant wall, the conductive heat flux through the wall from the hot-side to the cold-side, and the convective heat flux from the cold-side of the wall to the liquid coolant.

(c) The conduction heat transfer rate is expressed in terms of a constant thermal conductivity of the coolant wall material and the temperature difference between the hot and cold sides as:

$$Q_{hk} = \left(\frac{kA}{L}\right)(T_{w2} - T_{w1}) \tag{A.21}$$

where k is the coefficient of thermal conductivity, and A is the area of heat transfer.

(d) Convective heat transfer is associated with the mass transfer in a fluid boundary layer over a fixed wall. In. A.2, the rates of convective heat transfer Q_{gw} and Q_{wf} are given as:

$$Q_{gw} = h_c A(T_g - T_{w2}) \quad \text{from the hot gas to hot-side wall} \tag{A.22a}$$

$$Q_{wf} = h_c' A(T_{w1} - T_f) \quad \text{from the cold-side wall to coolant} \tag{A.22b}$$

Table A.5.—Main chamber and fixed nozzle regenerative cooling model equations

Main Chamber Regenerative Cooling Model Equations	**Fixed Nozzle Regenerative Cooling Model Equations**
$T_{CMW1} = \int_0^t \dot{T}_{CMW1}(t)dt + T_{CMW1}(0)$	$T_{NOZW} = \int_0^t \dot{T}_{NOZW}(t)dt + T_{NOZW}(0)$
$T_{CMW2} = \int_0^t \dot{T}_{CMW2}(t)dt + T_{CMW2}(0)$	$T_{NOZF} = \int_0^t \dot{T}_{NOZF}(t)dt + T_{NOZF}(0)$
$T_{CMBF} = \int_0^t \dot{T}_{CMBF}(t)dt + T_{CMBF}(0)$	
$Q_{CMBW} = C_{CMBWH}(T_{CMB} - T_{CMW2}) \times \lvert W_{CMB} \rvert^{0.8}$	$Q_{NOZW} = C_{NOZWH}(T_{NOZ} - T_{NOZW}) \times \lvert W_{NOZ} \rvert^{0.8}$
$C_{NOZFH} = C_{NOZFH}(1 + C_{NOZQ1}T_{NOZF})$	
$Q_{CMBWW} = C_{CMBK}(T_{CMW2} - T_{CMW1})$	
$Q_{CMBWF} = C_{CMBFH}(1 + C_{CMBQ1}T_{CMBF}) \times (T_{CMW1} - T_{CMBF}) \lvert W_{CMBF} \rvert^{0.8}$	$Q_{NOZWF} = C_{NOZFH}(T_{NOZW} - T_{NOZF}) \times \lvert W_{NOZF} \rvert^{0.8}$
$\dot{T}_{CMW2} = (Q_{CMBW} - Q_{CMBWW}) / C_{CMBWC}$	$\dot{T}_{NOZW} = (Q_{NOZW} - Q_{NOZWF}) / C_{NOZWC}$
$\dot{T}_{CMW1} = (Q_{CMBWW} - Q_{CMBWF}) / C_{CMBWC}$	
$\dot{T}_{CMBF} = (Q_{CMBWF} + W_{CMBF}C_{P,H_2} \times (T_{PMPE} - T_{CMBF})) / C_{CMBFC}$	$\dot{T}_{NOZWF} = (Q_{NOZWF} + W_{NOZF}C_{P,H_2} \times (T_{PMPE} - T_{NOZF})) / C_{NOZFC}$

where h_c is the convective heat transfer coefficient, T_{w2} and T_{w1} represent hot-side and cold-side wall temperatures, respectively, and T_f represents the bulk temperature of the liquid coolant. The convective heat transfer coefficient is described as a function of the fluid mass flow rate W and other system parameters at specified operating conditions using the following empirical correlation (Rockwell, 1989):

$$h_c \propto W^{0.8} \qquad \text{from the hot gas to hot-side wall} \tag{A.23a}$$

$$h_c \propto (1 + CT_f)W^{0.8} \qquad \text{from the cold-side wall to coolant} \tag{A.23b}$$

For a thermal system composed of a material of density ρ, specific heat c_p, and a constant volume V, the energy balance equation takes the following form:

$$\rho c_p V \frac{dT}{dt} = Q_{in}(t) - Q_{out}(t) + Q_{gen}(t) + \frac{\delta Work}{dt} \tag{A.25}$$

where Q_{in} or Q_{out} is the heat flux entering or exiting the control volume, Q_{gen} is the rate of heat generated within the control volume, and $\delta Work/dt$ is the time derivative of the work done upon the control volume.

Two wall temperatures at the two nodes on the hot and cold sides of the coolant channel wall, T_{CMBW} and T_{CMBWW}, and hydrogen coolant temperature, T_{CMBWF}, are the three state variables in the heat transfer model of the thrust chamber coolant channel. In reality, these state variables correspond to wall temperatures at the throat location where the heat flux is the highest and failure is most likely to occur. In contrast, the thrust chamber nozzle is relatively less prone to failure because of lower temperature. One lumped heat transfer node with two state variables is used to model the heat transfer through the nozzle coolant channel. The five state variables in the heat transfer model of the combustion and nozzle walls are:

- T_{CMW1} and T_{CMW2} are the cold-side and hot-side temperatures of the combustor wall.
- T_{CMBWF} and T_{NOZWF} are coolant fluid temperatures in the combustor and nozzle.
- T_{NOZW} is the average wall temperature of the nozzle.

Derivatives of wall temperatures, T_{CMW1}, T_{CMW2}, and T_{NOZW}, are obtained via Eq. (A.25) as:

$$\frac{d}{dt}(T_{CMW1}) = (Q_{CMBWW} - Q_{CMBWF})/C_{CMBWC} \tag{A.26a}$$

$$\frac{d}{dt}(T_{CMW2}) = (Q_{CMBW} - Q_{CMBWF})/C_{CMBWC} \tag{A.26b}$$

$$\frac{d}{dt}(T_{CMWF}) = \left[Q_{CMBWF} + W_{CMBF}C_{P,H_2}(T_{PMPE} - T_{CMBF})\right]/C_{CMBFC} \tag{A.26c}$$

The cold-side and hot-side temperatures, T_{CMW1} and T_{CMW2}, of the combustor wall are denoted as T_1 and T_2 for brevity in the creep damage model in Chapter 3. The model steady-state results are presented in Table A.6.

Table A.6.—Steady-state model results

Process Variables (State Variables)	Symbol	Unit	100% Model Results	Load Heat Balance
Fuel turbopump shaft speed	SPMP	rad/sec	3570.74	3577.6
Oxidizer turbopump shaft speed	SOPMP	rad/sec	2917.49	2849.4
Main thrust chamber hot-gas pressure	PCMB	psi	3000.0	3006.0
Main thrust chamber hot-gas density	RCMB	$lb/in.^3$	1.3358d-04	1.2673d-04
Fuel preburner hot-gas pressure	PPBR	psi	4831.0	4938.7
Oxidizer preburner hot-gas pressure	POPB	psi	4854.09	5003.5
Fuel preburner hot-gas density	RPBR	$lb/in.^3$	4.7846d-04	5.4478d-04
Oxidizer preburner hot-gas density	ROPB	$lb/in.^3$	6.4924d-04	6.7526d-04
Fuel flow rate into the fuel preburner	WHPBH	lb/sec	82.1055	78.18
Fuel flow rate into the oxidizer preburner	WOPBH	lb/sec	76.1259	67.78
Oxidizer flow rate into the fuel preburner	WHPBO	lb/sec	38.5659	35.1
Oxidizer flow rate into the oxidizer preburner	WOPBO	lb/sec	20.665	23.67
Oxidizer flow rate into the thrust chamber	WCMBO	lb/sec	809.656	801.77
Coolant side chamber wall temperature	TCMW1	°R	1240.43	/
Hot-gas side chamber wall temperature	TCMW2	°R	1457.45	/
Main thrust chamber coolant temperature	TCMBF	°R	483.341	469.1
Coolant side nozzle wall temperature	TNOZW	°R	1078.21	1260.0
Nozzle coolant temperature	TNOZF	°R	433.145	466.1
Fuel preburner oxygen flow valve position	AFPV	/	0.7813	0.7812
Oxidizer preburner oxygen flow valve position	AOPV	/	0.6387	0.6388

A.3 Simulation of Transient Responses of the Rocket Engine

In the thermo-fluid-dynamic model of the rocket engine derived above, the plant state vector consists of twenty state variables, two control inputs, and ten output variables as listed below:

State Variables:

Fuel Turbopump shaft speed	Oxidizer Turbopump shaft speed
Main thrust chamber hot-gas pressure	Main thrust chamber hot-gas density
Fuel preburner oxygen flow valve position	Oxidizer preburner oxygen flow valve position
Fuel preburner hot-gas pressure	Oxidizer preburner hot-gas pressure
Fuel preburner hot-gas density	Oxidizer preburner hot-gas density
Fuel flow rate into the fuel preburner	Fuel flow rate into the oxidizer preburner
Oxygen flow rate into the fuel preburner	Oxygen flow rate into the oxidizer preburner
Hot-side coolant wall temperature	Oxidizer flow rate into the main thrust chamber
Cold-side coolant wall temperature	Nozzle cooling tube wall temperature
Main thrust chamber coolant temperature	Nozzle coolant temperature

Control Inputs:

Fuel preburner oxidizer valve position	Oxidizer preburner oxidizer valve position

Output Variables for Life Prediction and Plant Control:

Main thrust chamber pressure	(O_2/H_2) mixture ratio
Fuel turbopump shaft speed	Oxidizer turbopump shaft speed
Fuel turbopump torque	Oxidizer turbopump torque

National Aeronautics and Space Administration
Lewis Research Center
Cleveland, Ohio 44135 August 20, 1997

References

Balas, G.J., et al.: μ-Analysis and Synthesis TOOLBOX. The Math Works, Inc., Natick, MA, 1993.

Bamieh, B.A.; and Pearson, J.B. Jr.: A General Framework for Linear Periodic Systems With Applications to H_∞ Sampled-Data Control. IEEE Trans. Automat. Contr., vol. 37, no. 4, April 1992, pp. 418–435.

Blackburn, J.F.; Reethof, G.; and Shearer, J.L.: Fluid Power Control, The M.I.T. Press, Cambridge, MA, 1960.

Dai, X.; and Ray, A.: Damage-Mitigating Control of a Reusable Rocket Engine: Parts I and II. J. Dyn. Syst. Meas. Control, vol. 118, no. 3, Sept. 1996, pp. 401–415.

Gill, P.E., et al.: User's Guide for NPSOL (Version 4.0): A Fortran Package for Nonlinear Programming. Stanford University Systems Optimization Lab, 1986.

Gill, P.E.; Murray, W.; and Wright, M.H.: Practical Optimization. Academic Press, New York, 1981.

Holmes, M.S.: Damage-Mitigating Control of Mechanical Systems, Ph.D. Dissertation, Department of Electrical Engineering, Pennsylvania State Univ., 1997.

Holmes, M.: and Ray, A.: Fuzzy Damage-Mitigating Control of Mechanical Structures. IEEE Conference on Decision and Control, San Diego, CA, Dec. 1997.

Holmes, M.; Tangirala, S.; and Ray, A.: Life Extending Control of Reusable Rocket Engines. J. Guid. Control and Dyn., May/June 1997, pp. 621–623.

Kallappa, P.; Holmes, M.S.; and Ray, A.: Life Extending Control of Fossil Power Plants. Automatica, vol. 33, no. 6, June 1997, pp. 1101–1108.

Lorenzo, C.F.: Continuum Fatigue Damage Modeling for Use in Life Extending Control. NASA TM–106691, 1994.

Lorenzo, C.F.; and Merrill, W.C.: An Intelligent Control System for Rocket Engines: Need, Vision, and Issues. Control Syst., vol. 11, Jan. 1991, pp. 42–46.

Lorenzo, C.F.; and Merrill, W.C.: Life Extending Control: A Concept Paper. NASA TM–104391, 1991.

Ray, A.; and Dai, X.: Damage-Mitigating Control of a Reusable Rocket Engine for High Performance and Extended Life. NASA CR–4640, 1995.

Ray, A., et al.: Damage-Mitigating Control of Mechanical Systems. Part I - Conceptual Development and Model Formulation. J. Dyn. Syst. Meas. Control, vol. 116, no. 3, Sept. 1994, pp. 437–447.

Ray, A., et al.: Damage-Mitigating Control of Mechanical Systems. Part II - Formulation of an Optimal Policy and Simulation. J. Dyn. Syst. Meas. Control, vol. 116, no. 3, Sept. 1994, pp. 448–455.

Rockwell International Corporation, Engine Balance and Dynamic Model. Report FSCM No. 02602, Spec. No. RL00001, Sept. 1981.

Schittkowski, K.: Software for Mathematical Programming. Proceedings of the NATO Advanced Study Institute on Computational Mathematical Programming, Springer-Verlag, 1984, pp. 383–451.

Sutton, G.P.: Rocket Propulsion Elements: An Introduction to the Engineering of Rockets. 6th ed., Wiley Interscience, New York, 1992.

Tangirala, C.: Stochastic Modeling of Fatigue Damage for On-line Monitoring, Prognostics and Life Extending Control, Ph.D. Dissertation, Department of Mechanical Engineering, Pennsylvania State Univ., 1996.

Vidyasagar, M.: Nonlinear Systems Analysis. Second ed., Prentice Hall, Englewood Cliffs, NJ, 1993.

Zhou, K.; Doyle, J.C.; and Glover, K.: Robust and Optimal Control, Prentice-Hall, Upper Saddle River, NJ, 1996.

REPORT DOCUMENTATION PAGE

Form Approved
OMB No. 0704-0188

1. AGENCY USE ONLY (*Leave blank*)	2. REPORT DATE	3. REPORT TYPE AND DATES COVERED
	April 1998	Technical Paper

4. TITLE AND SUBTITLE

Design of Life Extending Controls Using Nonlinear Parameter Optimization

5. FUNDING NUMBERS

WU-523-22-13-00

6. AUTHOR(S)

Carl F. Lorenzo, Michael S. Holmes, and Asok Ray

7. PERFORMING ORGANIZATION NAME(S) AND ADDRESS(ES)

National Aeronautics and Space Administration
Lewis Research Center
Cleveland, Ohio 44135-3191

8. PERFORMING ORGANIZATION REPORT NUMBER

E-10896

9. SPONSORING/MONITORING AGENCY NAME(S) AND ADDRESS(ES)

National Aeronautics and Space Administration
Washington, DC 20546-0001

10. SPONSORING/MONITORING AGENCY REPORT NUMBER

NASA TP-3700

11. SUPPLEMENTARY NOTES

Carl F. Lorenzo, NASA Lewis Research Center; Michael S. Holmes and Asok Ray, Pennsylvania State University, University Park, Pennsylvania 16802. Responsible person, Carl F. Lorenzo, organization code 5500, (216) 433-3733. Appendix-Thermo-Fluid Dynamic Modeling of the Reusable Rocket Engine by Asok Ray and Xuowen Dai taken from NASA CR-4650.

12a. DISTRIBUTION/AVAILABILITY STATEMENT

Unclassified - Unlimited
Subject Category: 63 Distribution: Standard

This publication is available from the NASA Center for AeroSpace Information, (301) 621-0390.

12b. DISTRIBUTION CODE

13. ABSTRACT (*Maximum 200 words*)

This report presents the conceptual development of a life extending control system where the objective is to achieve high performance and structural durability of the plant. A life extending controller is designed for a reusable rocket engine via damage mitigation in both the fuel and oxidizer turbines while achieving high performance for transient responses of the combustion chamber pressure and the O_2/H_2 mixture ratio. This design approach makes use of a combination of linear and nonlinear controller synthesis techniques and also allows adaptation of the life extending controller module to augment a conventional performance controller of a rocket engine. The nonlinear aspect of the design is achieved using nonlinear parameter optimization of a prescribed control structure.

14. SUBJECT TERMS

Life extending control; Damage; Damage mitigation; Nonlinear optimization

15. NUMBER OF PAGES

34

16. PRICE CODE

A03

17. SECURITY CLASSIFICATION OF REPORT	18. SECURITY CLASSIFICATION OF THIS PAGE	19. SECURITY CLASSIFICATION OF ABSTRACT	20. LIMITATION OF ABSTRACT
Unclassified	Unclassified	Unclassified	